Sliding-Window Correlation Attacks Against Encryption Devices with an Unstable Clock

Dor Fledel[1] and Avishai Wool[1]

School of Electrical Engineering, Tel-Aviv University, Tel-Aviv 69978, Israel
`dorfledel@tau.ac.il`, `yash@eng.tau.ac.il` ,
WWW home page: `https://www.eng.tau.ac.il/~yash/`

Abstract. Power analysis side channel attacks rely on aligned traces. As a counter-measure, devices can use a jittered clock to misalign the power traces. In this paper we suggest a way to overcome this counter-measure, using an old method of integrating samples over time followed by a correlation attack (Sliding Window CPA). We theoretically re-analyze this general method with characteristics of jittered clocks and show that it is stronger than previously believed. We show that integration of samples over a suitably chosen window size actually amplifies the correlation both with and without jitter — as long as multiple leakage points are present within the window. We then validate our analysis on a new data-set of traces measured on a board implementing a jittered clock. Our experiments show that the SW-CPA attack with a well-chosen window size is very successful against a jittered clock counter-measure and significantly outperforms previous suggestions, requiring a much smaller set of traces to correctly identify the correct key.

1 Introduction

1.1 Background

The use of encryption in embedded devices is proliferating. Encryption in such devices can be implemented in two ways, either by a hardware (ASIC or FPGA) implementation, or by software. Assuming that reasonable cryptographic algorithms are in use (e.g., AES), a cryptanalyst wanting to break the encryption can use side channel attacks (SCA), exploiting implementation-dependent information leakage captured during the cryptographic operation to find the correct key. A wide range of SCA exist, using leakage sources such as timing [Koc96], electromagnetic radiation [KA98], acoustic emanations [ST04] and even photonics [FH08]. Among these, one of the first and best understood SCA is power analysis. The idea of power analysis attacks is to perform statistical analysis of the CPU power usage, which is influenced by the secret cryptographic keys processed by the device. Some power analysis attacks assume profiling of the board, while others (non-profiling attacks) classify the behavior via a black-box methodology. Known non-profiling attacks such as Simple Power Analysis (SPA), traditional difference of means Differential Power Analysis (DPA) [KJJ99] and Correlation Power Analysis (CPA) [BCO04] are described in the literature and can be easily implemented by pre-made kits.

1.2 Power traces alignment: assumptions and counter-measures

Alignment assumption Power analysis SCA works by repeatedly sampling the power consumption of a device, while it is executing a cryptographic operation, using a high-speed oscilloscope and capturing multiple power traces. The main assumption is that the power consumption of certain instructions depends, in a statistical significant manner, on the secret key. Hence, by getting enough power traces and utilizing suitable analytical tools, one can extract the secrets.

A crucial property for the success of power SCA is that the power traces are *aligned*. Common power analysis attacks (i.e., DPA and CPA) assume that the information-leaking sub-step in the cryptographic implementation (for example an Sbox look-up) will always occur at a fixed interval after the power trace's beginning. If this assumption does not hold then the leaking information will appear at different offsets in different traces, which severely degrades the attack's ability to correlate the power leak to hypothetical key values.

Time domain hiding counter-measures One possible SCA counter-measure, originating in the initial days of power SCA (cf. [CCD00]) is "hiding in the time domain". This counter-measure breaks the assumption that traces are aligned. E.g., one variant of time domain hiding (dummy operations insertion) was analyzed by Mangard et al. [MOP08]. They showed that the correlation ratio between the correct key and the power consumption decreases, because not all traces leak in the same sample index.

Alignment problems have two common variants. In the first variant, the traces do not start at the same point, which can happen for example if there is no accurate trigger signal (start-point misalignment). In this case, the leaking encryption sub-state happens a fixed amount of time after the encryption start, but at a variable sample index within the trace after the measurement start. The second variant of misalignment, more commonly used by defenders, is that the encryption process itself has a variable time duration. Such behavior can be caused in many ways — insertion of random length dummy operations into the machine code execution, Random Process hardware Interrupts (RPIs) or an unstable (jittered) CPU clock. These methods lead to a leaking encryption sub-state happening at an uncertain point in time after the encryption start. Dummy operations insertion and RPIs cause the number of machine operations to be undetermined, whereas a jittered clock causes the execution time of these machine operations to be undetermined. E.g., A design for a jittered clock by Güneysu and Moradi [GM11] offers a CPU clock which is randomized by several independent clock buffers. Our focus in this paper is dealing with the jittered clock counter-measure.

1.3 Anti-counter-measures approaches to trace misalignment

For the variant of start-point misalignment, several possible solutions were suggested. Homma et al. [HNI$^+$06] suggested a method to align the traces according to trace properties in the frequency domain. Later, Schimmel et al. [SDB$^+$10] suggested Correlation Power Frequency Analysis (CPFA) which is impervious to start-point misalignment because frequency transform magnitude properties are independent of time domain shifting.

Batina et al. [BHvW12] proposed to solve the alignment problem by Principal Component Analysis (PCA). The method changes the possibly correlated linear base of the data-set to another linear uncorrelated base. This transformation may reveal a principal component which stands for the leakage. If such a component is found, there would be a correlation between its values and the correct key hypothesis, while the noise represented in other principal components is reduced. The authors did not suggest a way to predict the number of principal components required for the existence of leakage in these principal components.

The counter-measure variants involving a variable encryption length also have several solutions, typically via a pre-processing step. An early suggestion for time domain hiding was presented by Clavier et al. [CCD00], where the idea of samples integration in the pre-processing stage was introduced. Next, the authors proposed to perform a difference of means attack (traditional DPA), naming this method Sliding Window Differential Power Analysis (SW-DPA). The pre-processing involves aggregating several samples over number of consecutive cycles into one sample. For example, aggregating r out of each n samples for k cycles (creating a "comb-like" transformation). The integration was described as a solution for RPIs, without a specific parameter choosing suggestion. Later, to improve the performance after the pre-processing stage, a more efficient and powerful CPA attack was hinted by Brier et al. [BCO04]. Subsequently, this method was analyzed by Mangard et al. [MOP08]. Their analysis showed that when there is a single leaking sample among the r being aggregated, the correlation coefficient between the correct key hypothesis without jitter and the aggregated trace drops in proportion to $1/\sqrt{r}$; In other words, sliding-window aggregation seems to severely downgrade the performance of CPA.

Another proposed way to overcome the unstable clock counter-measure is to preform a traces alignment pre-processing step before the attack. Van Woudenberg et al. [vWWB11] suggested using the method of Dynamic Time Warping (DTW), and a DTW approximation called Fast DTW (FDTW), to align the traces according to one chosen reference trace, by minimizing the disparity. This alignment is done by modifying the aligned trace: inserting, deleting or matching sample points. However, the data-set used to evaluate the algorithm was created synthetically, by duplicating and deleting sampling points, hence the model in use might not be realistic. For example, if the device's power consumption is not constant within an instruction cycle (unstable noise amplitude), or if the clock's jittered frequencies are not divisible by the sampling frequency, then a large difference can be expected between the device's behavior and that of the authors' model. In their evaluation, the FDTW method outperformed two "straw-man" SW-DPA aggregation combinations. The two combinations of window size and number of windows were chosen while considering the instruction cycle length in samples and the "width" of the CPA correlation peaks. The results showed that choosing the window size and number of windows had a major impact on the results. The best results were achieved when the integration consisted of one continuous integration window rather than a "comb" with several distinct "teeth". The better performing SW-CPA parameters did not have an explanation in that article. Later, Muijrers et al. [MvWB11] showed a more computationally efficient way to align the traces using object recognition algorithms (Rapid Alignment Method). The experiments in the article were conducted on a case where random delays are added. This method is considered by the authors to be faster than FDTW but has similar detection results.

Conceptually simpler approaches were suggested in [TH12,HHO15]. Their algorithms were inspired by simple power analysis methods. They used the phenomena of traces' encryption round patterns that are sometimes observable in the traces for pre-processing. Hodgers et al. [HHO15] excluded high jitter traces from the data corpus by identifying peak-to-peak distances, while Tian et al. [TH12] made a specific efficient region alignment by identifying the encryption rounds.

Finally, hardware solutions were proposed for the jittered clock scenario, such as entangling the sampling clock and the board clock [OC15]. In this way, the attack is simple, while the measurement process overcomes the counter-measure. We argue that this idea seems quite difficult to use since the devices' clock is usually much harder to tap than the power supply.

In addition, there are more possible ways to handle alignment if one assumes full board access (profiling attacks). Such pre-processing approaches include, e.g., template attacks [CRR02] which require profiling of the board power consumption in advance, or reducing noise by linear transformations [OP12]. Other methods [CDP17] used machine learning and neural networks to attack several different time domain hiding countermeasures. Although these methods may have good results, and some might not be alignment dependent, we find their requirements to be challenging, and in this article we do not assume full control the board.

1.4 Contributions and structure

In this paper we suggest a new flavor of an old sliding-window attack to overcome the counter-measure of an unstable clock and we demonstrate that it works much better than predicted by earlier analysis. Extending the general notion of Clavier et al. [CCD00], we focus on the sliding-window aggregation of consecutive samples, followed by a correlation power analysis (CPA). We investigate how the attack performs without the assumption of a single leakage point for correlation calculations, and what are the best integration parameters. We start by revisiting the analysis of Mangard et al. [MOP08] and show that SW-CPA actually *amplifies* the correlation between the correct key hypothesis and the aggregated traces, both with and without jitter — as long as multiple leaking sample points are present in the integration window. We further show analytically that under mild conditions on the jitter model, there exist a choices of window sizes for which SW-CPA is very effective. Without jitter, for a single leakage point our analysis coincides with [MOP08]. However, our contribution is showing that with multiple leakage points in the window — integration amplifies the correlation for suitable choices of r. When jitter is present, both [CCD00,MOP08] and our work all show that integration drastically amplifies the correlation in comparison to using the raw unaligned traces. For multiple leakage points, we show that the integration method of [CCD00] with the correct parameter setting is more powerful than previously thought. This aspect of the analysis is validated by our experimental work.

Next, we evaluate the jitter introduced by a real commercial board which has a built-in spectrum-spreader. While this unstable clock was designed to reduce Electro-Magnetic Interference (EMI), we found it to be a powerful SCA counter-measure — its jittered traces caused severe degradation to standard CPA attacks. Through our evaluation we found that the board's jitter is in fact bounded. We then sampled the power consumption of the board while it executed a software implementation of AES, and collected a new corpus of power traces, both with and without jitter produced by the spectrum-spreader.

Then, we implemented a SW-CPA attack and conducted an extensive evaluation of its performance. We suggest a simple methodology to calibrate the size of the integration window. We also compare the predictions of our analytical model to the empirical performance of SW-CPA and demonstrated a good match: for the chosen integration window sizes multiple leaking samples are present in the window. The method indeed amplified the correlation and was able to revert the impact of the unstable clock almost completely.

Finally, We compared the performance of SW-CPA to that of several previously suggested SCA on our real-life data corpus: SW-CPA clearly outperformed prior attacks, requiring a vastly smaller number of traces to achieve the same level of secret key detection.

Organization: Section 2 introduces the jittered clock counter-measure and the SW-CPA attack. Section 3 theoretically analyzes the attack and predicts its effectiveness under some mild assumptions on the leakage and the jitter model. Section 4 describes the experiments we conducted with our jittered clock setup and the validation of our analytical model. Section 5 discusses the SW-CPA attack and compares it with other state-of-the-art methods. Section 6 gives final conclusions.

2 The effect of an unstable clock on standard attacks

2.1 Unstable CPU clock and time domain hiding analysis

An unstable clock (i.e., jittered clock) is a technique in which the CPU does not have a constant clock frequency, but one which can fluctuate in a given frequency domain. When the clock is unstable, the cryptanalyst attempting SCA is not certain any more that the leaking signal measurements occur in the same point in time — at the same sample index in the trace (see Figure 1).

As shown in [MOP08], CMOS circuits have data dependent power consumption called dynamic power consumption. This dynamic power consumption is

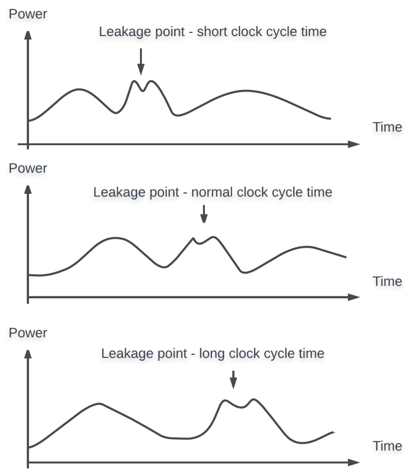
Power
Leakage point - short clock cycle time
Time
Power
Leakage point - normal clock cycle time
Time
Power
Leakage point - long clock cycle time
Time

Fig. 1: CPU power consumption vs. time, for different traces with different clock frequencies

a dominant factor in the board's total power consumption. It occurs when the cell needs switching for digital signal transition. A CMOS cell's switching power consumption is proportional to the clock frequency:

$$P_{switching} \propto f_{CPU}$$

When the frequency of the board changes, the amount of data dependent power leakage also changes. However, for our analysis we shall assume that the different CPU clock frequencies are close to each other, and do not have a significant effect on the power consumption model.

2.2 Basic time domain hiding analysis:

Following [MOP08], let P, P_{orig} be the random variables representing the board's instantaneous power consumption at sample index t_0, with and without the hiding counter-measure respectively. These random variables represent the power consumption over the different traces at a point in time in which the leak occurs. We use the leaking Hamming weight model commonly used in SCA against software encryption implementations. Let H_i denote the random variable representing the power consumption estimation for hypothetical key byte value i. Each different known plaintext input combined with key byte value i results in a specific data Hamming weight during encryption sub-states. Due to Hamming weight behavior, H_i are normally distributed random variables. Let H_{ck} be the random variable representing the hypothetical power consumption of the correct

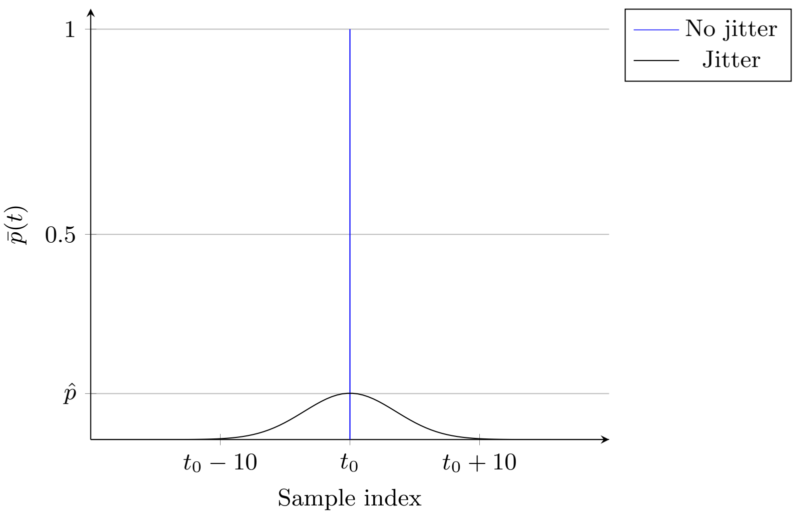

Fig. 2: The probability of a leakage point position in the trace at sample points near the original leakage point t_0 as a function of the sample index, without and with jitter (sample drift normally distributed).

key byte value. Let $\rho(H_{ck}, P)$ denote the Pearson correlation coefficient between these random variables.

Assume that P_{orig} is computed at sample index t_0. When jitter is present, the leak that occurs at time t_0 drifts due to hiding, meaning the observation of the leak may not be at sample t_0, but might be within a range of sample indexes, either before or after t_0. We denote the probability of the leak occurring in a specific sample index t by $\bar{p}(t)$. Let $\hat{p}$ denote $\max_t \bar{p}(t)$. We assume that $\hat{p}$ is achieved at the same sample index t_0 that would likely contain the most of leakage points over the different traces, thus having the highest correlation ratio. This idea is illustrated in Figure 2, comparing the non-jittered case where there is certainty about the leakage sample index, and the jittered case with an example of normally distributed drift values.

For aligned power traces without jitter, $\hat{p} = 1$ because the leakage points all occur in the same sample number. However, for misaligned power traces $\hat{p} \neq 1$, and the maximal correlation ratio between the observed power consumption P and the correct key hypothetical power consumption H_{ck} would be:

$$\rho(H_{ck}, P) = \rho(H_{ck}, P_{orig}) \cdot \hat{p} \tag{1}$$

2.3 Sliding Window CPA attack on jittered CPU clocks

The Sliding Window Differential Power Analysis attack (SW-DPA) was initially proposed in [CCD00]. It was proposed as a way to eliminate the counter-measure of RPIs insertion for random delays with aggregation parameters similar to a

Algorithm 1 Sliding Window Correlation Power Analysis Attack (SW-CPA)

```
1: procedure PreprocessTrace(Trace, r)
2:     for $t \in Trace$ do
3:         $SummedTrace(t) = \sum_{i=-r/2}^{r/2} Trace(t+i)$
4:     return SummedTrace
5: procedure Attack(r)
6:     Acquire set of traces $X$
7:     for $Trace \in X$ do
8:         $Trace \leftarrow PreprocessTrace(Trace, r)$.
9:     Perform CPA on X.
```

"comb" function transformation. The original attack was performed with traditional difference of means DPA (single bit model attack).

Our attack on jittered CPUs, which we call the Sliding Window Correlation Power Analysis attack (SW-CPA), is inspired by [CCD00]; we use a similar pre-processing idea but then we use a CPA attack (byte model attack). Furthermore, unlike the example in [CCD00], we use only a single continuous integration window with a size of r (aggregating r consecutive samples instead of a sparse "comb" aggregation) — see Algorithm 1. The attack exploits the fact that although each trace's leakage can happen at a different time due to jitter, with a high probability the leakages will occur within some radius $r/2$ of the original leakage sample point (without the counter-measure). If we then apply the CPA attack on the integrated traces, there would be a common trace sample index containing the leakage for many different traces. We chose to aggregate one continuous window (rather than the comb-like integration of [CCD00]) as we cannot assume, without profiling, where the leakage would be, and we would like the drifted leakage points to be included within the integrated window.

2.4 Basic correlation analysis of sliding-window integration

To begin with, let us find the Pearson correlation coefficient of a key hypothesis with the pre-processed traces data-set, when no jitter is present and the traces are aligned. Without loss of generality assume that a leakage occurs at sample point 1. Let ρ_1 be the correlation coefficient between the leakage sample P_1 and the correct key hypothesis H_{ck}. Then, by definition we have:

$$\rho_1 \equiv \rho(H_{ck}, P_1) = \frac{Cov(H_{ck}, P_1)}{\sqrt{Var(H_{ck}) \cdot Var(P_1)}} = \frac{E(H_{ck} \cdot P_1) - E(H_{ck}) \cdot E(P_1)}{\sqrt{Var(H_{ck}) \cdot Var(P_1)}} \quad (2)$$

In [MOP08] pp. 210-211, Mangard et al. analyzed the effect of the integration of r independent power samples, $\{P_{-r/2}, \dots, P_1, \dots, P_{r/2}\}$, containing exactly a single leakage sample. Their analysis shows that:

$$\rho(H_{ck}, \sum_{i=-r/2}^{r/2} P_i) = \frac{\rho_1}{\sqrt{r}} \quad (3)$$

Equation (3) is clearly an upper bound on the correlation once jitter is introduced. Therefore, under the analyzed conditions there is a trade-off on setting the window size r. On the one hand, when we increase r, we increase the likelihood that the leakage sample would be within our aggregation window because the drift value caused by jitter will be smaller than r. Consequently, due to Equation (1), we would like to increase the window size. On the other, Equation (3) seems to show that integration decreases the correlation by the square root of the window size, which would force the cryptanalyst to use many more traces to compensate.

3 A new analysis of multiple leakage samples integration

The conclusion from [MOP08] as seen in Equation (3) is that when using integration, the samples' noise is aggregated, and the correlation ratio drops. In this section we show that on the contrary, SW-CPA integration can be an effective technique which actually *amplifies* the correlation with and without jitter. We do this by using a different and very realistic model of the leakage observed in the power traces. In Section 4 we validate that our model assumptions indeed hold on traces collected from a real device with a jittered clock.

3.1 The correlation coefficient when integrating within a trace

The leakage model previously mentioned in Section 2.4 assumes only a *single* leakage point within the integration window, and $r-1$ power samples independent of the encryption key (non leakage samples). However, there might be several leakage samples in a trace. Whenever the cryptanalyst observes more than one peak in the correlation coefficient in a CPA for the correct key byte, there is more than one leakage point. This may be caused by several reasons: multiple leakage sources may exist, such as data bus leakage, address bus leakage or different electronic components' glitches which may all happen sequentially. Alternatively, a high sampling frequency of the measurement instrument may cause switching to spread over more than one sample. CPU architecture and software implementation may imply more phenomena creating such behavior. For example, Papagiannopoulos et al. [PV17] showed that the data might be loaded to several registers during the computation. As we shall see, in traces we collected (without jitter), we observed this phenomenon quite clearly: there were multiple leak points, relatively close to each other in time.

We start our analysis with the case of aligned traces: we assume the clock is stable and analyze the effect of SW-CPA with different values of window size r.

Assume that among the r samples $\{P_{-r/2}, \ldots, P_1, \ldots, P_{r/2}\}$, there are $q(r) \geq 1$ leakage points and $r - q(r)$ samples independent of the correct key hypothesis H_{ck} (which we call for short "noise samples"). For the $q(r)$ leakage samples, we assume that the random variables P_i are identically distributed but not independent since they all depend on the leak — but their variability is caused by the noise, which we can reasonably argue to be independent among different sample points. Therefore, they have the same expectation and variance. Without loss of generality, assume that P_1 is a leakage sample point, so for all $q(r)$ leakage samples P_i, P_j, $(i \neq j)$ we have:

$$\begin{aligned} E(P_i) &= E(P_1) \\ Var(P_i) &= Var(P_1) \end{aligned} \tag{4}$$

By definition for two leakage samples with same variance, using Pearson correlation coefficient $\rho_{i,j}$ between power samples P_i, P_j, we have:

$$Cov(P_i, P_j) \equiv \sqrt{Var(P_i) \cdot Var(P_j)} \cdot \rho_{i,j} = Var(P_1) \cdot \rho_{i,j} \tag{5}$$

For the other $r - q(r)$ noise samples we can safely assume that they are independent of each other and of the leakage points. Therefore, for samples P_i, P_j where at least one is a noise samples, we get that P_i and P_j are uncorrelated, i.e., $Cov(P_i, P_j) = 0$.

Next, we assume that while the expectations of the key-dependent and noise samples are different, they all have the same variance, since they are all subject to the same noise, i.e.,

$$Var(P_i) = Var(P_1) \text{ for all } i.$$

Hence, for all samples, regardless of the sample type (leakage or noise), we conclude that for all P_i , P_j:

$$Cov(P_i, P_j) = \begin{cases} Var(P_1) \cdot \rho_{i,j} & i, j \text{ are leakage samples} \\ 0 & \text{Otherwise} \end{cases} \tag{6}$$

The noise samples are also independent of the correct key hypothesis (because they are not leakage points), so for such sample P_i:

$$E(H_{ck} \cdot P_i) = E(H_{ck}) \cdot E(P_i) \tag{7}$$

Now we return to the correlation coefficient. According to Equation (2), the correlation coefficient for r integrated samples is:

$$\rho(H_{ck}, \sum_{i=-r/2}^{r/2} P_i) = \frac{E(H_{ck} \cdot (\sum_{i=-r/2}^{r/2} P_i)) - E(H_{ck}) \cdot E(\sum_{i=-r/2}^{r/2} P_i)}{\sqrt{Var(H_{ck}) \cdot Var(\sum_{i=-r/2}^{r/2} P_i)}} =$$

$$\frac{\sum_{i=-r/2}^{r/2} (E(H_{ck} \cdot P_i) - E(H_{ck}) \cdot E(P_i))}{\sqrt{Var(H_{ck})) \cdot Var(\sum_{i=-r/2}^{r/2} P_i)}}$$

We know there are exactly $q(r)$ leakage samples. Separating the sums for key byte leakage and noise indexes, Equations (4) and (7) and the standard formula for the variance of a sum give:

$$\rho(H_{ck}, \sum_{i=-r/2}^{r/2} P_i) = \frac{q(r) \cdot (E(H_{ck} \cdot P_1)) - E(H_{ck}) \cdot E(P_1))}{\sqrt{Var(H_{ck})} \cdot \sqrt{\sum_{i=-r/2}^{r/2} Var(P_i) + \sum_{i \neq j} Cov(P_i, P_j)}}$$

By Equation (6) and plugging in the definition of ρ_1 (non-jittered correlation without integration) from Equation (2) we can simplify the result to:

$$\rho(H_{ck}, \sum_{i=-r/2}^{r/2} P_i) = \frac{q(r) \cdot (E(H_{ck} \cdot P_1) - E(H_{ck}) \cdot E(P_1))}{\sqrt{Var(H_{ck})} \cdot \sqrt{r + \sum_{i \neq j} \rho_{i,j}} \cdot \sqrt{Var(P_1)}} \implies$$

$$\rho(H_{ck}, \sum_{i=-r/2}^{r/2} P_i) = \frac{q(r)}{\sqrt{r + \sum_{i \neq j, \text{leakage samples}} \rho_{i,j}}} \cdot \rho_1 \tag{8}$$

Let γ denote the normalized sum of correlation coefficients of the leakage points:

$$\gamma \equiv \frac{r + \sum_{i \neq j, \text{leakage samples}} \rho_{i,j}}{r}$$

Then, we can rewrite Equation (8) as:

$$\rho(H_{ck}, \sum_{i=-r/2}^{r/2} P_i) = \frac{q(r)}{\sqrt{r \cdot \gamma}} \cdot \rho_1 \tag{9}$$

If all the leakage points are uncorrelated samples then $\rho_{i,j} = 0 \Rightarrow \gamma = 1$. Conversely, in the worst case the leakage points are fully correlated with $\rho_{i,j} = 1 \Rightarrow \gamma = r$. Because γ is derived from the correlation matrix of random variables, it is positive semidefinite and in particular the sum of its items is non-negative, hence also $\gamma \geq 0$. However, γ can be smaller than 1 causing a further amplification. Casting Equation (9) to also explicitly show the interesting cases we get

$$\rho(H_{ck}, \sum_{i=-r/2}^{r/2} P_i) = \begin{cases} \frac{q(r)}{\sqrt{r}} \cdot \rho_1 & \text{uncorrelated leakage samples} \\ \frac{q(r)}{\sqrt{r \cdot \gamma}} \cdot \rho_1 & \text{partly correlated leakage samples} \\ \frac{q(r)}{r} \cdot \rho_1 & \text{fully correlated samples} \end{cases} \tag{10}$$

For simplicity, unless mentioned otherwise, in the derivations below we assume leakage samples are uncorrelated, hence:

$$\gamma = 1 \tag{11}$$

As we shall see in Section 4.3, in the data we gathered γ is quite close to 1 and much smaller than r.

We can see that for the special case of $q(r) = 1$ we get exactly Equation (3), i.e., the result of Mangard et al. [MOP08]. For the most special case, where $r = q = 1$ we obtain the standard CPA attack.

3.2 Correlation coefficient amplification:

Let P_t be the distribution of trace power values at sample index t. Let

$$\rho_{cpa} = \max_t \rho(H_{ck}, P_t)$$

be the achieved correlation coefficient of a regular CPA attack on the traces. Now, assume we conduct a SW-CPA with a window size of r. Then let

$$\rho_r = \max_t \rho(H_{ck}, \sum_{i=-r/2}^{r/2} P_{t+i})$$

be the correlation achieved by SW-CPA with window size r. Note that $\rho_{cpa} \equiv \rho_1$. Both ρ_1 and ρ_r should have similar jitter properties (or no jitter). We define the correlation coefficient *amplification* to be:

$$\mathit{Amplification} = \rho_r / \rho_1$$

The cryptanalyst's goal is to maximize the amplification, to reveal as many secret key bytes as possible.

3.3 The correlation coefficient for specific r and q relationships

Equation (10) can be made concrete if we have an explicit connection between r and q. We first assume that each key byte has a maximal number of leakage points, q_{max}. Further, we assume that all q_{max} leakage points are temporally close: they are all located within a distance of r_0 samples from each other. Therefore, when $r \geq r_0$ the window is called saturated and q stops growing with r. So we get:

$$q = \begin{cases} q(r) & \text{if } r < r_0 \\ q_{max} & \text{otherwise (saturation)} \end{cases} \tag{12}$$

With this assumption we analyze two important cases:

Constant number of leakage points In case $r \geq r_0$, our window contains all q_{max} leakage points of the phenomenon. Increasing the window size any further does not change the value of q. According to Equation (10), the correlation would be:

$$\rho(H_{ck}, \sum_{i=-r/2}^{r/2} P_i) = \frac{q_{max}}{\sqrt{r}} \cdot \rho_1 \tag{13}$$

Hence, when r increases ρ decreases, and for $r > q_{max}^2$ the correlation drops below ρ_1 and eventually $\rho \to 0$. Therefore, a cryptanalyst who seeks to maximize ρ, should select the value of r to be the smallest possible value containing all q_{max} leakage points.

This observation is also valid for the general case. When the number of leakage points $q(r)$ does not change while incrementing r, the correlation decreases by $\sqrt{r}$ until more leakage points are aggregated into the integration window.

Constant ratio between r and q Another important case is when the integration window is not saturated, and increasing r increases the number of leakage points q *linearly* such that $q(r) = r/c$ for some constant c. In this case:

$$\rho(H_{ck}, \sum_{i=-r/2}^{r/2} P_i) = \frac{q(r)}{\sqrt{r}} \cdot \rho_1 = \frac{r/c}{\sqrt{r}} \cdot \rho_1 \implies$$

$$\rho(H_{ck}, \sum_{i=-r/2}^{r/2} P_i) = \frac{\sqrt{r}}{c} \cdot \rho_1 \tag{14}$$

The first implication of this equation is that when $\sqrt{r} > c$ we obtain that $\rho > \rho_1$: in other words, without jitter, not only does integration not reduce the correlation coefficient, it can even amplify it. However, as we increase r, eventually the number of leakage points saturates, yielding a non constant ratio between r and $q(r)$ and we fall back to Equation (13).

Therefore, according to Equations (13) and (14), we get that the relationship between ρ, the correlation coefficient of the integrated non-jittered traces; r, the window size; q, the number of leakage points within the window; and c, the ratio between r and q is:

$$\rho(H_{ck}, \sum_{i=-r/2}^{r/2} P_i) = \begin{cases} \frac{\sqrt{r}}{c} \cdot \rho_1 & r < r_0, \text{constant ratio between } q \text{ and } r \\ \\ \frac{q_{max}}{\sqrt{r}} \cdot \rho_1 & r \geq r_0 \text{ (saturated } q) \end{cases} \tag{15}$$

Still assuming for simplicity that $\gamma = 1$.

3.4 The correlation coefficient with an unstable clock

So far, our analysis of SW-CPA assumed a stable clock and aligned traces. When we use an unstable clock, the correlation coefficient is also affected by the probability that the leakage signals happen in the window around the same point in time, as stated in Equation (1). We denote by $\hat{q}(r)$ the number of leakage points in a window of size r when jitter is present.

Combining $\hat{q}$ leakage points and the case of uncorrelated samples in Equation (10) yields the general correlation coefficient for the jittered clock:

$$\rho(H_{ck}, \sum_{i=-r/2}^{r/2} P_i) = \frac{\hat{q}(r)}{\sqrt{r}} \cdot \rho_1 \tag{16}$$

The correlation coefficient of bounded jitter We now assume the clock jitter is bounded and the maximal drift that a logical action in the encryption process can suffer is J sample points (we validate our assumption empirically in

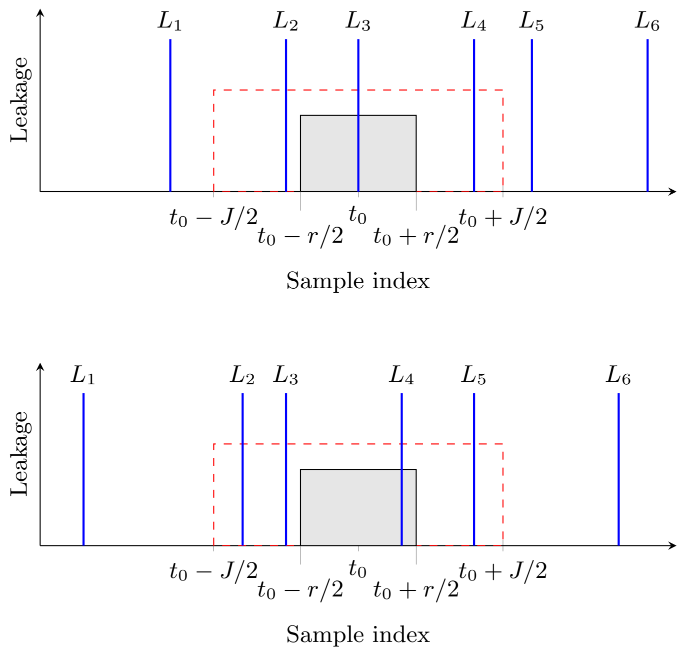

Fig. 3: Leakage vs. sample index for two specific traces. Blue lines are leakage points. The red dashed line is the possible drift region around t_0. The gray area is the integration window around t_0. The upper sub-figure is non-jittered while the lower sub-figure has jitter. The drift for the original L_3 leakage point caused it to fall outside the window while L_4 falls into the window.

Section 4.2). We seek to find the relation between $\hat{q}$ and q for different values of r. It is important to notice that the drift might change between different traces and different samples in the data-set.

For simplicity, we assume that the drift of a sample point is uniformly distributed in time around the original non-jittered index, i.e., $Drift \sim U\{\frac{-J}{2}, \frac{J}{2}\}$.

Because the drift is distributed uniformly and $E(Drift) = 0$, the distance between the leakage points might increase as well as decrease, but it's expectation is equal to the non-jittered case.

Figure 3 gives a schematic example for leakage samples, their drift over time, and how the number of leakage samples in the window is affected. We can see that although the original leakage point drifted, another leakage point was integrated in the window.

Recall that r_0 denotes the window size such that all q_{max} leakage samples are in the window. Hence, with jitter, we take a worst-case scenario and assume that the q_{max} leakage points are distributed uniformly among the $r_0 + J$ samples. Further, saturation happens in a larger window size because of the drift.

Therefore we get:

$$\hat{q}(r) = \begin{cases} \frac{q_{max}}{r_0+J} \cdot r & \text{if } r < r_0 + J \\ q_{max} & \text{otherwise (saturation)} \end{cases} \tag{17}$$

The CPA correlation coefficient in the jittered case We first calculate $\hat{\rho_1}$, the correlation coefficient for original CPA attack ($r = 1$) with jitter $J > 1$. The leakage signal originally always happens at t_0, but due to the jitter it may occur anywhere within the range $[t_0 - J/2, t_0 + J/2]$.

According to Equation (17), the probability that a leakage point appears in sample index t_0 is:

$$\hat{q}(r = 1) = \frac{q_{max}}{r_0 + J} = \frac{r_0}{r_0 + J} \cdot \frac{1}{c} \tag{18}$$

due to the uniform leakage distribution.

Putting Equations (16) and (18) together gives the correlation ratio for the standard CPA ($r = 1$) against jittered traces:

$$\hat{\rho_1} = \frac{\hat{q}(r = 1)}{\sqrt{r}} \cdot \rho_1 = \frac{r_0}{r_0 + J} \cdot \frac{1}{c} \cdot \rho_1 \tag{19}$$

We can see that according to Equation (19), when jitter is present the standard CPA attack effectiveness is severely degraded — as we shall see in Section 5.2.

The SW-CPA Correlation coefficient for different r values We now analyze two important cases of r, caused by the different domains of $\hat{q}$ in Equation (17), under the effect of a bounded jitter.

Constant q/r ratio: When $r < r_0 + J$ from Equations (16) and (17), the correlation coefficient for SW-CPA is:

$$\rho(H_{ck}, \sum_{i=-r/2}^{r/2} P_i) = \hat{q}(r) \cdot \frac{1}{\sqrt{r}} \cdot \rho_1 = \frac{q_{max} \cdot r}{r_0 + J} \cdot \frac{1}{\sqrt{r}} \cdot \frac{r_0 + J}{r_0} \cdot c \cdot \hat{\rho_1} \implies$$

$$\rho(H_{ck}, \sum_{i=-r/2}^{r/2} P_i) = \sqrt{r} \cdot \hat{\rho_1} \tag{20}$$

Saturated $\hat{q}$ values: The region around t_0 when $r \geq r_0 + J$ contains all the leakage points, meaning $\hat{q}(r) = q_{max}$. Combining Equations (16) and (19) gives for $r \geq r_0 + J$:

$$\rho(H_{ck}, \sum_{i=-r/2}^{r/2} P_i) = \frac{\hat{q}(r)}{\sqrt{r}} \cdot \rho_1 = \frac{q_{max}}{\sqrt{r}} \cdot \frac{r_0 + J}{r_0} \cdot c \cdot \hat{\rho_1} = \frac{r_0 + J}{\sqrt{r}} \cdot \hat{\rho_1} \tag{21}$$

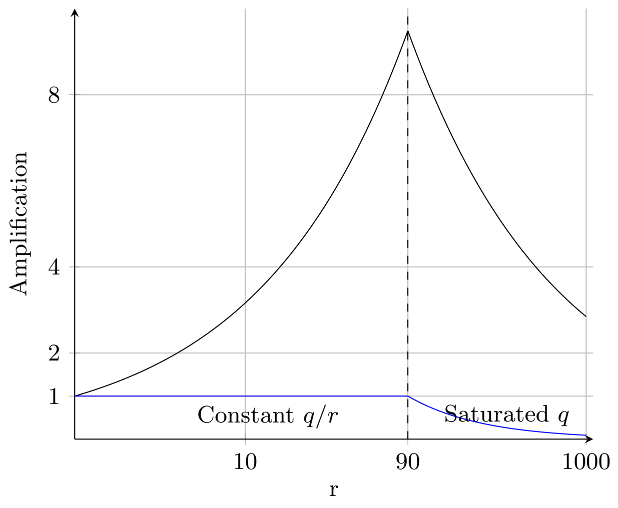

Fig. 4: SW-CPA attack amplification of correlation coefficient (with jitter) vs. window size r (log scale) for $J = 20$, $r_0 = 70$. The black line is the scenario for uncorrelated leakage samples ($\gamma = 1$). The blue line is for the worst case correlated leakage samples ($\gamma = r$). The dashed line at $r = 90$ separates the two regions of the amplification (constant q/r ratio and saturated q). Amplification values above 1 indicate that ρ is amplified beyond the values for $r = 1$ (CPA attack on a jittered clock data-set).

Summarizing Equations (20) and (21), we get that the relationship between ρ, the correlation coefficient of the integrated jittered traces; $\hat{\rho_1}$, the correlation coefficient without integration; r, the window size; q, the number of leakage points within the window; c, the ratio between r and q; replugging in the equation of γ from Equation (10); and J, the maximal drift is:

$$\rho(H_{ck}, \sum_{i=-r/2}^{r/2} P_i) = \begin{cases} \frac{\sqrt{r}}{\sqrt{\gamma}} \cdot \hat{\rho_1} & r < r_0 + J, \text{constant ratio between } q \text{ and } r \\ \\ \frac{r_0+J}{\sqrt{r}\sqrt{\gamma}} \cdot \hat{\rho_1} & r \geq r_0 + J \text{ (saturated } q) \end{cases} \tag{22}$$

Figure 4 illustrates Equation (22). The parameter values in this figure were chosen according to the values found later in our experimental part (see Section 5.1). The upper curve models a bounded jitter for uncorrelated leakage ($\gamma = 1$) where $J = 20$, $r_0 = 70$, $c = 3$ (leakage in a third of the samples in the window), and q reaches saturation of $q_{max} = 25$ when $r = r_0 + J = 90$. Note that under these conditions the SW-CPA can amplify the correlation ratio by factor of 10 when $r = 90$. The Figure also illustrates the worst case scenario where the leakage samples are all fully correlated and $\gamma = r$, where we can see no amplification.

The correlation coefficient with an unbounded jitter While our analysis assumed that the jitter is bounded (and in Section 4.2 we demonstrate this is a realistic assumption for our board), we argue that our analysis has merit in more general cases as well. Even if the jitter is unbounded we still expect to observe a randomly changing clock frequency according to some distribution. In such a case, we assume that using a reasonable clock spreading model, it should be possible to build a sample drift model in which with high probability the drift value would be in a specific range, thus making our analysis relevant. We leave the analysis of cases with unbounded jitter to future work.

4 Experiments and results

4.1 Setup and measurements

Our experimental setup centers around a Rabbit RCM4010 evaluation board. This device has a 59MHz processor with a 16-bit architecture [RCM10]. We programmed the board to implement an AES-128 algorithm using open-source code taken from [Con12]. This is a plain-vanilla software implementation of AES, without any side channel counter-measures or software optimizations (i.e., without using T-tables).

The Rabbit processor has a special feature called a spectrum-spreader — designed to reduce electromagnetic interference (EMI). Enabling the spreader introduces jitter into the CPU clock frequency. However, the documentation does not specify precisely how the spectrum-spreader works. Note that the Rabbit has two spreading modes, called Normal and Strong (in addition to no spreading mode), which can be selected by software. Our main experiments used the Normal mode, but additional experiments were conducted with Strong jitter and showed similar results.

We sampled the board power by a Lecroy WavePro 715Zi oscilloscope. When starting the execution of an encryption, we programmed the board to send a signal to the oscilloscope via one of its I/O pins which can be controlled by the software. This signal sets the trigger for the oscilloscope, which starts sampling at a rate of 500 million samples per second, for 500μs. This time period contains one round of the full AES encryption. Every encryption process is recorded to a new trace. The voltage of the processor was measured by a shunt resistor soldered to the processor voltage input. The input plaintexts for the program were changed every encryption round, while the key was kept constant during all traces. Two data-sets where captured; one consisted 5,000 traces without jitter and 5,600 traces with Normal jitter, using the same encryption key and plaintexts (for the first 5,000 jittered traces). The second and bigger data-set contains 10,000 traces of each spectrum-spreading mode: no spreading, Normal spreading and Strong spreading. These measurements were done with a different random key than the first data-set, but same plaintexts.

Note that while the spectrum-spreader is not an SCA counter-measure by design, we found it to be quite effective as such. E.g., as we shall see in Section 5.2,

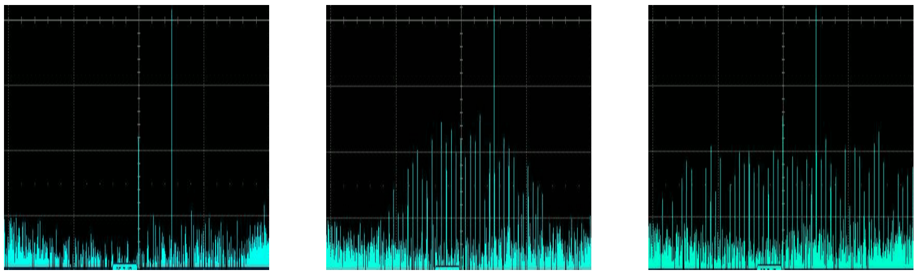

(a) Without jitter (b) Normal jitter (c) Strong jitter

Fig. 5: FFT magnitude vs. frequency of the power trace from RCM board, computed by the oscilloscope (a) without jitter, (b) with Normal jitter, (c) with Strong jitter, centered around 59MHz (original clock frequency) and axis between 55-63 MHz

when the spectrum-spreader is turned on, the standard CPA attack is drastically degraded: without jitter the attack correctly discovers all 16 key bytes with as few as 2,500 traces, while with jitter CPA fails to identify more than two key bytes even with all 5,600 traces of the first data-set.

4.2 Jitter modeling

We first explored the jitter injected by the spectrum-spreader to validate the analysis of Section 3.4. This part was used for white-box validation of our leakage model only and is not essential for the common adversary. When spectrum-spreading was enabled, frequency analysis revealed several new frequencies that appeared around the original 59MHz clock frequency, with about 0.15MHz difference between them. Figure 5(a) shows the spectrum without jitter: notice the peaks at 59MHz and 60MHz (the former is the board clock frequency). Figure 5(b) shows the spectrum with Normal jitter: notice how the 59MHz peak is replaced by some 15-25 separate peaks while the irrelevant 60MHz peak is unaffected. Figure 5(c) shows the spectrum with Strong jitter: some 15 additional peaks appeared with higher and lower frequencies.

Next, we conducted a set of experiments in order to understand the drift of the jittered clock (Normal jitter). We programmed the board to implement the following steps (see Algorithm 2): send a first signal to the oscilloscope, then perform N times a condition test and a variable assignment, and finally send a second signal when finishing the execution. The time between the two signals (ΔT) was saved and analyzed. We set the execution length N to start at about a quarter of the total AES encryption time ($N = 600 \implies \Delta T = 2ms$), and increased it to more than the encryption time ($N = 3000 \implies \Delta T = 10ms$). We also tested intermediate values of $\Delta T = 4ms$ and $\Delta T = 5ms$. 500 executions were done for each of the N values. When spectrum-spreading was not enabled, ΔT was identical in all executions (per execution length).

Algorithm 2 Drift assessment

```
1: procedure PerformInstructions(N)
2:     Send an initial signal for execution start
3:     for $i$ from 1 to $N$ do
4:         if $True$ then
5:             $Var1 \leftarrow 0$
6:     Send a second signal for execution end
```

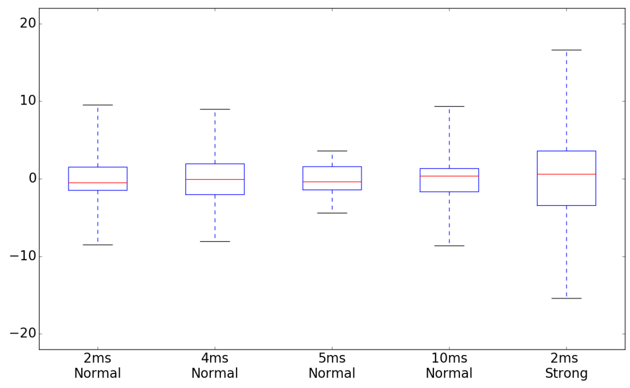

Fig. 6: Drift in number of samples (D) vs. different execution duration (ΔT) with the Normal and Strong spectrum-spreader. The red line is the median, the bottom and top of the boxes represent the first the third quartiles, and the whiskers range from the minimum to the maximum samples drift. Normal spreading is bounded by $|D| = 10$ samples and Strong spreading is bounded by $|D| = 20$ samples.

When Normal spreading was enabled ΔT was not constant per execution length. We denote by D the difference, in number of samples, between the execution length with jitter and the constant execution length without jitter. For different execution lengths, we observed that the magnitude of the drift ($|D|$) was *bounded* by at most 10 samples ($20ns$) to each side, regardless of the execution length. Using the terminology of Section 3.4, the Rabbit Normal spectrum-spreader has a bound $J = 20$, $|D| = 10$. Similar experiments with the Strong spectrum-spreader showed that the drift is still bounded but with $J = 40$, $|D| = 20$. The bounded drift in number of samples is illustrated by a box plot in Figure 6, for both Normal spreading and Strong spreading (box plots for additional Strong spreading execution lengths omitted).

We believe that drift is not accumulating beyond $|D| = 10$ for Normal spreading and $|D| = 20$ for Strong spreading because the spreading is probably generated by a fixed cyclic series of clock jitter values, with a cycle time shorter than $2ms$. The bounded drift is consistent with the board design, since even a short

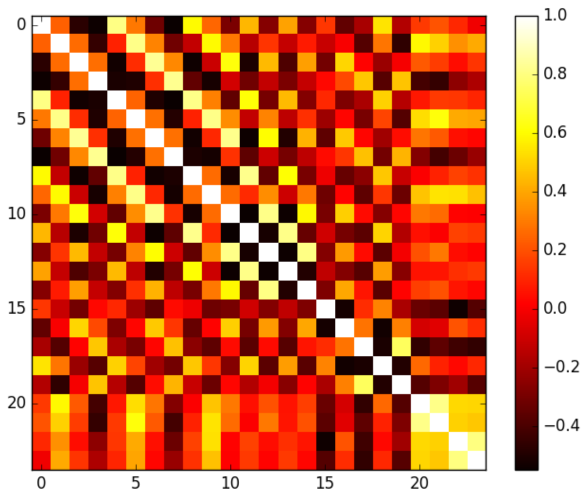

Fig. 7: Correlation matrix heat-map, for 25 leakage sample points for the best leakage window of key byte 7

cycle of jitter values can achieve the goal of EMI reduction, much more easily than generating true random, or cryptographic pseudo-random, clock jitter.

4.3 Validating leakage points' power consumption correlation

Next, we need to validate our assumptions in Equations (4), (6) and (10) about the distributions and correlation between leakage points and the value of γ. In Figure 7 we show a heat-map of the correlation coefficients between 25 leakage sample points of a specific key byte, for 5,000 traces without jitter. These leakage samples form the best window for integration with maximal correlation between the true key byte and the traces as shown in Section 5.2. In order to find the leakage points, we set a threshold (of 3 standard deviations above or below the mean) over the correlation coefficient of a sample index to differentiate between leakage and noise samples. Figure 7 shows that the off-diagonal correlations are both negative and positive: these sign alternations in fact help keep the total correlation low, with a total sum of $\gamma = 1.7$ (including diagonal values). Thus, the correlation coefficient in Equation (10) is divided by $\sqrt{\gamma} = 1.3$, which is still highly amplified in comparison to CPA without integration. This experiment was done for all key bytes, resulting in γ values between 0.5 to 1.7 with average 0.95 and standard deviation of 0.33 — supporting our assumption in Equation (11) that γ is close to 1; hence we can treat the leakages as if they are uncorrelated without a great penalty in the analysis.

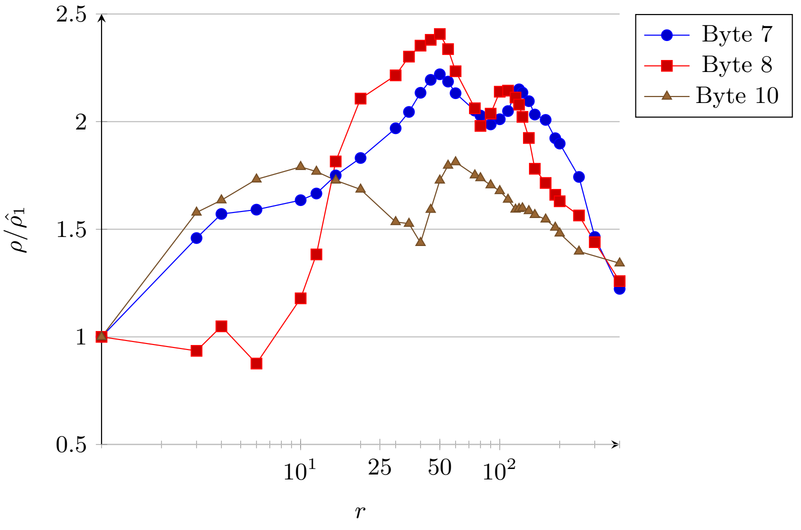

Fig. 8: Amplification of the correlation coefficient vs. window size r (log scale), for three correct key bytes, with the jittered clock data-set of 5,600 traces. Amplification values above 1 indicate that ρ is amplified beyond the values for $r = 1$.

5 Evaluating the SW-CPA attack

5.1 Amplification for different aggregation window sizes

To calibrate the best window size r we examined leaks from the different key bytes in our encryption process. Figure 8 shows the amplification of the correlation coefficient for different window sizes and different correct key bytes when the CPU clock is jittered. Note that these key bytes are not identified correctly by CPA without pre-processing due to jitter. For simplicity, we do not show all key bytes.

The amplification graphs for all key bytes have major similarities. First, they all have an amplification higher than 1 for some window size r, which helps the correct key byte detection and supports SW-CPA as an effective solution for the unstable clock counter-measure. In addition, they all suffer degradation when r grows beyond a certain point and q reaches saturation. Finally, we see that the amplification does not increase monotonically toward a single peak — unlike the prediction in Figure 4. We explore this issue below.

Note that some of the curves contain a significant peak when r is relatively small, around $5 \leq r \leq 10$, as demonstrated in key byte 10. This is somewhat surprising because as stated in Equation (22), for a small window size r, the integration might not be as effective as for a large window size. We speculate that maybe the leaks for some key bytes had statistically repetitive drift values or a small number of leakage points with a relatively dense scatter. Another option is that the leakage samples are correlated in a way that γ is relatively small for this small window of leakage samples.

5.2 Selecting a window size r for all key bytes

Next, we determine the single, best, r value of all key bytes for our device. Figure 9 shows the overall SW-CPA success rate for different r values together with the results for standard CPA on non-jittered traces (as an ideal) and CPA on the jittered traces (as a worst-case).

The metric we used to recognize a correct key byte detection counted a correct key byte when the true key byte was within the highest five correlation possibilities, i.e., the key byte recovery is of the 5th order as stated in [SMY09]. This metric was chosen because a cryptanalyst can iterate (brute force) over the remaining $5^{16} \approx 2^{37}$ options.

We've experimentally seen in Figure 8 that the ρ amplification graphs for separate key bytes had the highest peaks between $25 < r < 75$. We chose the overall value of $r = 75$ experimentally, without profiling information, simply by running the attacks.

Figure 9 shows clearly that SW-CPA is very effective attack and defeats the clock jitter counter-measure well: for values of $10 \leq r \leq 75$ it finds 12-14 correct key bytes with ≈ 4500 traces — only twice as many traces as needed for an equivalent success rate on non-jittered traces. Further, we see that our attack is not very sensitive to the value of r: values between $10 \leq r \leq 75$ are roughly equally successful. The figure shows that a larger window such as $r = 150$ gives a poor amount of true key byte detections. Window sizes below $r = 10$ have inferior performance (graphs omitted).

Figure 10 shows similar results for a larger data-set (10,000 traces) with a different key and Strong spectrum-spreading. The figure shows that SW-CPA is very successful against Strong jitter as well: it correctly finds all key bytes, with about 6,000 traces, for many window sizes, whereas regular CPA cannot find two correct key bytes even with all 10,000 traces. In addition, the higher drift with Strong jitter causes SW-CPA with large window size such as $r = 300$ to be effective and find 15-16 key bytes, whereas with Normal spreading (Figure 9) $r = 150$ was already too high and performance was degraded in comparison to $r = 75$.

To determine the optimal window size r, we suggest choosing its value after analyzing the q/r ratio for all key bytes if possible, or otherwise by trial and error (no profiling). Choosing an imprecise value of r still gives far better results than other state-of-the-art methods as would be shown later: Even for clearly sub-optimal choices of r our method is superior to others (see Figure 11). In addition, the computational resources for trial and error are low in comparison to other methods. Furthermore, one might also use a different window size for each key byte. We did not explore this possibility since the results with a uniform r were satisfactory.

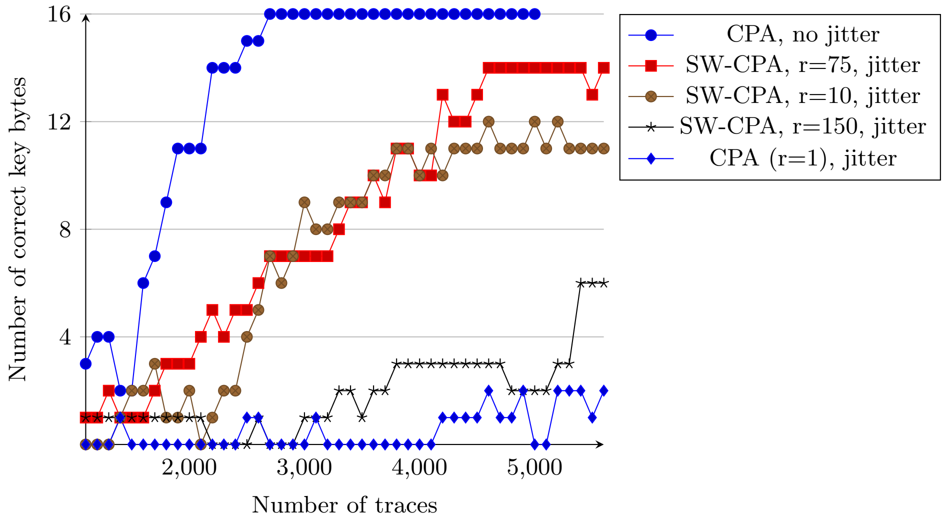

Fig. 9: Number of correct key bytes vs. number of traces, for different values of the integration window size r and Normal Jitter

5.3 Comparing SW-CPA with other known methods

We compare the SW-CPA method (with the best integration window size) to previously suggested methods: trace selection pre-processing [HHO15], alignment pre-processing [TH12,vWWB11,BHvW12], and frequency analysis attacks [SDB$^+$10]. Figure 11 summarizes the results.

Applying the methods suggested in [HHO15,TH12] of pre-processing according to simple trace properties was inapplicable to our data-set. These attacks were originally performed on hardware encryption implementations and assume that the power consumption measurements have clearly visible patterns of the AES rounds. Our data with a software implementation on the Rabbit board exhibited no such patterns. We tried searching for the patterns with different sampling frequencies and different number of samples but the expected 10 spikes marking the 10 AES rounds did not manifest themselves in the power traces. A possibility why we did not observe the patters is that the Rabbit board we used is not idle between the encryption cycles or when waiting for input. Because the attacks rely on the visible encryption rounds, the device cannot be attacked by these methods.

Another available solution is using a PCA attack [BHvW12]. As mentioned before, this attack works if there exists a principal component representing the leakage. However, in our base transformations, no such principal component was found, even with high numbers of base items and concentrating in the leakage region of the traces.

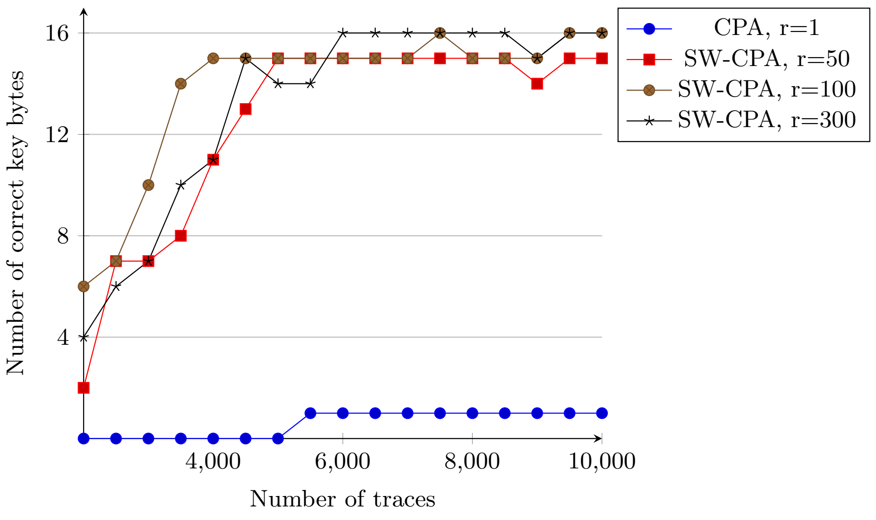

Fig. 10: Number of correct key bytes vs. number of traces, for different values of the integration window size r and large data-set with Strong spectrum-spreading.

Therefore, the methods of pre-processing according to simple trace properties and PCA [HHO15,TH12,BHvW12] detected zero key bytes correctly, and were not inserted to the comparison in Figure 11.

The method of elastic alignment [vWWB11] did not give us a high percentage of correct key byte detection either (as was also observed by others who tested it with non-simulated data-sets [OP11,GPPT15]). The original article [vWWB11] offers a way to overcome the computational complexity of DTW by using FDTW, which is an approximation for DTW. We first implemented and tested FDTW with poor results. After FDTW failed, we applied the full DTW (with just the relevant alignment margin because of our bounded jitter) which slightly improved the results. Figure 11 shows the results of the improved DTW implementation.

The method of Correlation Power Frequency Analysis (CPFA) [SDB+10] was previously offered as a method for handling the start-point misalignment, because the magnitude in the frequency domain is not affected by time domain shifting. The results of this method were poor as well. We tried to optimize this attack as well, by targeting leakage areas, but results stayed the same.

Comparison to SW-DPA was more challenging. Clavier et al. [CCD00] did not suggest a way to determine their algorithm's parameters, hence we do not see how to compare their general approach to our specific instantiation. However, their SW-DPA with 1-bit difference of means using our integration parameters gave poor results and was omitted from the comparison figure.

For the SW-CPA attack, Figure 11 shows the result with the window size $r = 75$, found in Section 5.2. Many other choices of r still outperform other methods as well.

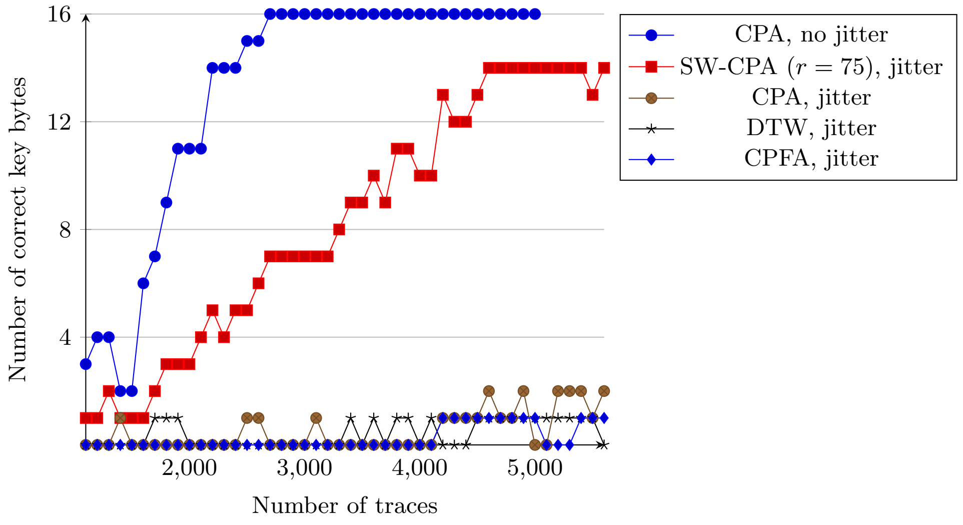

Fig. 11: Number of correct bytes vs. number of traces, for different implemented attacks. Attacks with 0 key bytes successfully detected were omitted. We also show the success rate of the standard CPA attack on non-jittered data (as an ideal).

Figure 11 clearly shows that SW-CPA yields far better true key byte detection results than the other possible solutions we tried. All the other solutions did not have more than two correct key bytes detections on our data-set with 5,600 traces. However, note that the unstable clock still degregates the attack: even our best SW-CPA requires approximately twice the number of traces to achieve an equivalent level of success in comparison to standard CPA against a non-jittered device.

6 Conclusions

In this paper we suggested an attack to overcome the jittered CPU clock counter-measure, proposing a specific parameter setting for the old method of consecutive samples integration followed by a correlation attack (Sliding Window CPA). Former analysis showed that integration of samples degrades the correlation between the correct key hypothesis and the trace. We re-analyzed this method under a new model where multiple leakage points may be present within the window, and we showed that integration of samples over a suitably chosen window size amplifies the correlation significantly. We then validated our analysis on a new data-set of traces measured on a board implementing a jittered clock. Our experiments show that the SW-CPA attack with the optimal window size is very powerful against a jittered clock counter-measure and significantly outperforms previous state-of-the-art suggestions.

References

BCO04. Eric Brier, Christophe Clavier, and Francis Olivier. Correlation power analysis with a leakage model. In *Cryptographic Hardware and Embedded Systems (CHES)*, pages 16–29. Springer, 2004.

BHvW12. Lejla Batina, Jip Hogenboom, and Jasper GJ van Woudenberg. Getting more from PCA: First results of using principal component analysis for extensive power analysis. In *CT-RSA*, volume 7178, pages 383–397. Springer, 2012.

CCD00. Christophe Clavier, Jean-Sébastien Coron, and Nora Dabbous. Differential power analysis in the presence of hardware countermeasures. In *Cryptographic Hardware and Embedded Systems (CHES)*, pages 13–48. Springer, 2000.

CDP17. Eleonora Cagli, Cécile Dumas, and Emmanuel Prouff. Convolutional neural networks with data augmentation against jitter-based countermeasures. In *International Conference on Cryptographic Hardware and Embedded Systems (CHES)*, pages 45–68. Springer, 2017.

Con12. Brad Conte. Basic implementations of standard cryptography algorithms, like AES and SHA-1, 2012. `https://github.com/B-Con/crypto-algorithms`.

CRR02. Suresh Chari, Josyula R Rao, and Pankaj Rohatgi. Template attacks. In *International Workshop on Cryptographic Hardware and Embedded Systems (CHES)*, pages 13–28. Springer, 2002.

FH08. Julie Ferrigno and M Hlaváč. When AES blinks: introducing optical side channel. *IET Information Security*, 2(3):94–98, 2008.

GM11. Tim Güneysu and Amir Moradi. Generic side-channel countermeasures for reconfigurable devices. *Cryptographic Hardware and Embedded Systems (CHES)*, pages 33–48, 2011.

GPPT15. Daniel Genkin, Lev Pachmanov, Itamar Pipman, and Eran Tromer. Stealing keys from PCs using a radio: Cheap electromagnetic attacks on windowed exponentiation. In *International Workshop on Cryptographic Hardware and Embedded Systems (CHES)*, pages 207–228. Springer, 2015.

HHO15. Philip Hodgers, Neil Hanley, and Maire O'Neill. Pre-processing power traces to defeat random clocking countermeasures. In *International Symposium on Circuits and Systems (ISCAS)*, pages 85–88. IEEE, 2015.

HNI$^+$06. Naofumi Homma, Sei Nagashima, Yuichi Imai, Takafumi Aoki, and Akashi Satoh. High-resolution side-channel attack using phase-based waveform matching. In *Cryptographic Hardware and Embedded Systems (CHES)*, pages 187–200. Springer, 2006.

KA98. Markus G Kuhn and Ross J Anderson. Soft tempest: Hidden data transmission using electromagnetic emanations. In *Information hiding*, volume 1525, pages 124–142. Springer, 1998.

KJJ99. Paul Kocher, Joshua Jaffe, and Benjamin Jun. Differential power analysis. In *Advances in cryptology (CRYPTO)*, pages 789–789. Springer, 1999.

Koc96. Paul C Kocher. Timing attacks on implementations of Diffie-Hellman, RSA, DSS, and other systems. In *Annual International Cryptology Conference*, pages 104–113. Springer, 1996.

MOP08. Stefan Mangard, Elisabeth Oswald, and Thomas Popp. *Power analysis attacks: Revealing the secrets of smart cards*, volume 31, pages 202–211. Springer Science & Business Media, 2008.

MvWB11. Ruben A Muijrers, Jasper GJ van Woudenberg, and Lejla Batina. RAM: Rapid alignment method. In *International Conference on Smart Card Research and Advanced Applications (CARDIS)*, pages 266–282. Springer, 2011.

OC15. Colin O'Flynn and Zhizhang Chen. Synchronous sampling and clock recovery of internal oscillators for side channel analysis and fault injection. *Journal of Cryptographic Engineering*, 5(1):53–69, 2015.

OP11. David Oswald and Christof Paar. Breaking MILFARE DESFIRE MF3ICD40: Power analysis and templates in the real world. In *Cryptographic Hardware and Embedded Systems (CHES)*, pages 207–222. Springer, 2011.

OP12. David Oswald and Christof Paar. Improving side-channel analysis with optimal linear transforms. In *International Conference on Smart Card Research and Advanced Applications*, pages 219–233. Springer, 2012.

PV17. Kostas Papagiannopoulos and Nikita Veshchikov. Mind the gap: Towards secure 1st-order masking in software. In *IACR Cryptology ePrint Archive*, page 345, 2017.

RCM10. Digi International Inc. RabbitCore RCM4000 user manual, 2010. `http://ftp1.digi.com/support/documentation/019-0157_J.pdf`.

SDB$^+$10. Oliver Schimmel, Paul Duplys, Eberhard Boehl, Jan Hayek, R Bosch, and W Rosenstiel. Correlation power analysis in frequency domain. In *COSADE First International Workshop on Constructive Side Channel Analysis and Secure Design*, 2010.

SMY09. François-Xavier Standaert, Tal Malkin, and Moti Yung. A unified framework for the analysis of side-channel key recovery attacks. In *Eurocrypt*, volume 5479, pages 443–461. Springer, 2009.

ST04. Adi Shamir and Eran Tromer. Acoustic cryptanalysis. 2004. presentation available from `http://www.wisdom.weizmann.ac.il/~tromer`.

TH12. Qizhi Tian and Sorin A Huss. On the attack of misaligned traces by power analysis methods. In *Computer Engineering & Systems (ICCES), 2012 Seventh International Conference on*, pages 28–34. IEEE, 2012.

vWWB11. Jasper GJ van Woudenberg, Marc F Witteman, and Bram Bakker. Improving differential power analysis by elastic alignment. In *Cryptographers Track at the RSA Conference*, pages 104–119. Springer, 2011.